Journal of Animal Environment

(E-ISSN 2717-1396, ISSN 2717-1388)

Original Research Paper

Green synthesis and characterization of Lawsonia inermis-mediated Au-Ag bimetallic nanoparticles: in-vitro antioxidant activity and preliminary in-vivo evaluation in an ICV-STZ mouse model

Rajkumari Lodhi, Dr. Virendra Kumar Sharma*

School of Pharmacy, LNCT University, Bhopal, Madhya Pradesh, India 462042
Corresponding author: **Dr. Virendra Kumar Sharma** dr.virendra48@gmail.com
School of Pharmacy, LNCT University, Bhopal, Madhya Pradesh, India 462042
Research Scholar: **Rajkumari Lodhi** keshrajkumari5521@gmail.com
School of Pharmacy, LNCT University, Bhopal, Madhya Pradesh, India 462042

Abstract

Alzheimer's disease (AD) is associated with progressive cognitive decline, oxidative stress, neuroinflammation, and amyloid-related pathology. This study investigated the green synthesis and physicochemical characterization of gold-silver bimetallic nanoparticles (Au-AgNPs) using an aqueous leaf fraction of Lawsonia inermis, assessed their in-vitro antioxidant activity, and integrated preliminary in-vivo findings from an intracerebroventricular streptozotocin (ICV-STZ) mouse model. Synthesis conditions were optimized by varying extract volume, precursor concentration, pH, and temperature. The optimized preparation used 100 µL extract, 1 mM metal precursor, pH 7, and 30 °C and displayed a surface-plasmon-resonance band near 537 nm. FT-IR indicated changes in plant-associated functional groups, XRD and SAED supported a crystalline face-centred cubic structure, EDX detected both Au and Ag, and HR-TEM showed particles approximately 10-32 nm in size. Au-AgNPs showed concentration-dependent in-vitro activity, reaching 88.78% DPPH, 90.03% hydrogen-peroxide, and 88.08% nitric-oxide scavenging at 100 µg/mL. In the supplied ICV-STZ dataset, Au-AgNP treatment was associated with cholinesterase activity, hippocampal cytokine concentrations, and cholesterol values closer to healthy-control values. Some animal-protocol details and biomarker results were incomplete in the source material and require verification. These data support further investigation but do not establish cognitive efficacy, definitive nose-to-brain targeting, or efficacy of an in-situ gel formulation. Complete safety, pharmacokinetic, brain-distribution, behavioural, and reproducibility studies are needed.

Keywords: Lawsonia inermis; Au-Ag bimetallic nanoparticles; green synthesis; optimization; antioxidant activity; HR-TEM; nose-to-brain delivery; Alzheimer's disease; nanotechnology.

Introduction

Alzheimer's disease (AD) is a chronic and progressive neurodegenerative disorder and one of the major causes of dementia worldwide. The disease is characterized by progressive deterioration of memory, cognition, behavior, and the ability to perform daily activities [1-3]. The major pathological hallmarks of AD include extracellular accumulation of amyloid-β (Aβ) plaques and intracellular formation of neurofibrillary tangles composed primarily of hyperphosphorylated tau protein. These pathological alterations are accompanied by oxidative stress, mitochondrial dysfunction, chronic neuroinflammation, synaptic impairment, and progressive neuronal loss [4-7]. Although considerable progress has been made in understanding the molecular mechanisms underlying AD, effective treatment remains challenging. A major obstacle in the treatment of neurological disorders is the blood-brain barrier (BBB), which restricts the penetration of many therapeutic molecules into the central nervous system. Consequently, drugs administered through conventional oral or parenteral routes may exhibit inadequate concentrations at the target site [8-9]. Furthermore, first-

***Corresponding Author:**
Received: 25th May, 2026; Revised: 6th July, 2026; Accepted: 28th July, 2026; Available Online: 29th August, 2026
(DOI): 10.70102/AEJ.2026.18.8s.22

pass metabolism, systemic distribution, enzymatic degradation, and peripheral adverse effects may further limit therapeutic efficacy. These challenges have stimulated considerable interest in alternative drug-delivery strategies capable of improving drug transport to the brain [10].

Intranasal administration has emerged as a promising non-invasive approach for central nervous system drug delivery. The nasal cavity provides anatomical connections with the brain through the olfactory and trigeminal pathways, potentially allowing certain therapeutic molecules and nanocarriers to reach the central nervous system while partially circumventing the BBB [11-14]. Intranasal administration may therefore improve brain exposure and reduce systemic drug exposure. However, rapid mucociliary clearance and the relatively short residence time of conventional nasal formulations may limit drug absorption and therapeutic performance [15].

Nanotechnology offers several opportunities to overcome these limitations. Nanoparticles can improve the solubility, stability, protection, and controlled release of therapeutic agents and may facilitate interaction with biological barriers. Among different nanosystems, bimetallic nanoparticles have received increasing attention because they combine the physicochemical characteristics of two metals within a single nanoscale system. Depending on their composition, morphology, particle size, surface chemistry, and synthesis method, bimetallic nanoparticles may exhibit enhanced optical, catalytic, antimicrobial, antioxidant, and other biological properties compared with their monometallic counterparts.

Gold (Au) and silver (Ag) are two extensively investigated noble metals for nanoparticle synthesis. Combining Au and Ag may produce nanoparticles with distinctive physicochemical properties resulting from interactions between the two metals. However, the biological activity and safety of such nanoparticles depend strongly on their size, morphology, surface chemistry, composition, concentration, and method of synthesis. Therefore, controlled synthesis and comprehensive characterization are essential before considering biomedical applications [16-18].

Green synthesis of nanoparticles using plant extracts has emerged as an environmentally friendly alternative to conventional physical and chemical synthesis methods. Plant-derived phytochemicals, including phenolic compounds, flavonoids, proteins, terpenoids, sugars, and other reducing molecules, can participate in the reduction of metal ions and stabilization of the resulting nanoparticles. This approach may reduce the requirement for harsh chemical reducing agents and provide biologically functionalized nanoparticle surfaces[19-20].

Lawsonia inermis L. (henna) is a medicinal plant traditionally used for various therapeutic and cosmetic applications. Its leaves contain several classes of phytochemicals, including phenolic compounds, flavonoids, tannins, and other bioactive constituents. These compounds may provide reducing and stabilizing properties during nanoparticle synthesis while potentially contributing to the biological activity of the resulting nanoparticles [10].

In the present investigation, an aqueous fraction of L. inermis leaf extract was employed for the green synthesis of Au-Ag bimetallic nanoparticles. The synthesis conditions were systematically optimized by investigating the effects of extract volume, metal precursor concentration, pH, and temperature. The optimized nanoparticles were characterized using UV-Visible spectroscopy, FT-IR, XRD, EDX, HR-TEM, and SAED. Furthermore, their antioxidant potential was investigated using DPPH, H_2O_2, and NO radical scavenging assays, reducing power, and total phenolic content.

The overall objective was to establish a reproducible green synthesis approach for Au-Ag bimetallic nanoparticles with defined physicochemical characteristics and antioxidant potential. These findings may provide a basis for subsequent development of nanoparticle-based delivery systems, including intranasal formulations intended for nose-to-brain delivery. However, the latter application requires independent formulation-development and biological validation studies.

2. Materials and Methods

2.1. Collection and Processing of Lawsonia inermis Leaves

Fresh leaves of Lawsonia inermis were collected from the local area of Bhopal, Madhya Pradesh, India. The collected leaves were thoroughly washed with running tap water followed by triple-distilled water to remove adhering dust and other surface contaminants. The cleaned leaves were allowed to dry at room temperature for approximately 2 h under conditions protected from direct sunlight. The leaves were subsequently cut into coarse pieces using a laboratory blender and used for solvent extraction.

2.2. Preparation of L. inermis Leaf Extract

Approximately 200 g of processed L. inermis leaves were transferred into a 1000-mL round-bottom flask and successively extracted using solvents of increasing polarity. The solvents used were n-hexane, chloroform, ethyl acetate, methanol, and water. Each extraction was performed separately under reflux at 80 °C for 1 h using a reflux condenser. Following extraction, the respective extracts were filtered through Whatman No. 1 filter paper. The filtrates were concentrated under reduced pressure using a rotary evaporator to obtain the corresponding solvent fractions. The dried fractions were collected separately and stored at 4 °C until further investigation. The solubility of the obtained fractions was assessed in water and dimethyl sulfoxide (DMSO), where appropriate, before preliminary phytochemical analysis.

2.3. Preliminary Phytochemical Screening and Preparation of Extract and Metal Precursor Solutions

***Corresponding Author:**
Received: 25th May, 2026; Revised: 6th July, 2026; Accepted: 28th July, 2026; Available Online: 29th August, 2026
(DOI): 10.70102/AEJ.2026.18.8s.22

The n-hexane, chloroform, ethyl acetate, methanol, and aqueous fractions of Lawsonia inermis leaves were subjected to preliminary qualitative phytochemical screening to identify the major classes of secondary metabolites using standard procedures described by Sofowora, Trease and Evans, and Harborne [5-7]. The aqueous fraction of L. inermis leaf extract (AF-LSE) was subsequently used as the biological reducing and stabilizing agent for bimetallic nanoparticle synthesis. For stock solution preparation, 50 mg of AF-LSE was accurately weighed, dissolved in triple-deionized water, and diluted to a final volume of 10 mL. Separately, 39.383 mg of $HAuCl_4$ and 16.987 mg of $AgNO_3$ were dissolved individually in 100 mL of triple-deionized water to prepare 1 mM gold and silver precursor solutions, respectively. Finally, the prepared $HAuCl_4$ and $AgNO_3$ solutions were mixed in a 1:1 volume ratio to obtain the Au-Ag metal precursor solution for the synthesis of bimetallic nanoparticles.

2.4. Preliminary Synthesis and Optimization of Au-Ag Bimetallic Nanoparticles

The preliminary synthesis of gold-silver bimetallic nanoparticles (Au-Ag BNPs) was performed by mixing an appropriate volume of Lawsonia inermis aqueous leaf extract (AF-LSE) with the metal precursor solution at room temperature. A visible color change in the reaction mixture was considered a preliminary indication of metal-ion reduction and nanoparticle formation. The synthesis process was subsequently optimized by systematically investigating the effects of extract volume, metal precursor concentration, pH, and temperature, with nanoparticle formation and stability monitored using UV-Visible spectroscopy. The effect of extract volume was evaluated by adding 10, 50, 100, 150, and 200 µL of AF-LSE stock solution to 5 mL of 1 mM Au-Ag metal precursor solution. The effect of precursor concentration was studied using concentrations of 0.5, 1, 2, 3, and 4 mM, with 100 µL of AF-LSE added to 5 mL of each solution. The influence of pH was investigated over the range of 5-9 by adjusting the pH of the reaction mixtures using 0.01 M HCl or 0.01 M NaOH, followed by the addition of 100 µL of AF-LSE to 5 mL of 1 mM Au-Ag precursor solution. Furthermore, the effect of temperature was examined at 15, 30, 50, 70, and 80 °C using 100 µL of AF-LSE and 5 mL of 1 mM Au-Ag precursor solution. The reaction mixtures were maintained under the respective experimental conditions, protected from light where specified, and monitored by UV-Visible spectroscopy at predetermined time intervals to identify the conditions favoring nanoparticle synthesis**.**

2.5. Synthesis of Au-Ag BNPs under Optimized Conditions

Based on the optimization studies, the conditions providing favorable nanoparticle formation and spectral stability were selected. The optimized synthesis was performed using 100 µL of AF-LSE stock solution and 5 mL of 1 mM Au-Ag metal precursor solution at pH 7 and 30 °C. The reaction mixture was sonicated for 10 min using an ultrasonic bath operating at 40 kHz with a maximum power of 100 W. A progressive color change of the reaction mixture was observed during nanoparticle formation.

2.6. Characterization of Au-Ag Bimetallic Nanoparticles

2.6.1. UV-Visible Spectroscopy

The optical properties and formation of Au-Ag BNPs were investigated using a PerkinElmer Lambda 25 UV-Visible spectrophotometer. The absorption spectra were recorded over the wavelength range of 200-800 nm using triple-deionized water as the blank. The progress of nanoparticle formation was monitored at different reaction times by recording the corresponding UV-Visible spectra. The appearance and stability of the surface plasmon resonance (SPR) band were used to evaluate nanoparticle formation.

2.6.2. Fourier-Transform Infrared Spectroscopy

FT-IR spectroscopy was performed to investigate the functional groups of the plant extract involved in the reduction and stabilization of Au-Ag BNPs. The synthesized nanoparticles were centrifuged at 8000 rpm for 10 min. The resulting nanoparticle pellet was separated, washed with deionized water to remove unbound constituents, and dried at 50 °C for 24 h. The dried material was mixed with KBr and compressed into pellets. FT-IR spectra were recorded using a JASCO FT-IR spectrometer over the range of 4000-400 cm^{-1}.

2.6.3. X-Ray Diffraction Analysis

The crystalline characteristics of the synthesized Au-Ag BNPs were investigated using a PANalytical X'PERT-PRO powder X-ray diffractometer. The analysis was performed using Cu-Kα radiation at 40 kV and 30 mA. Diffraction patterns were recorded over an appropriate 2θ range. The crystalline phases were identified from the characteristic diffraction peaks, and the average crystallite size was estimated using the Scherrer equation.

2.6.4. Energy-Dispersive X-Ray Spectroscopy

EDX analysis was performed to determine the elemental composition of the synthesized Au-Ag BNPs. The nanoparticle sample was analyzed using an EDS X-ray spectrometer coupled with a ZEISS EVO 18 scanning electron microscope system. The characteristic elemental signals corresponding to Au and Ag were used to confirm the elemental composition of the synthesized bimetallic nanoparticles.

2.6.5. High-Resolution Transmission Electron Microscopy

HR-TEM was performed to investigate the morphology and size distribution of the synthesized Au-Ag BNPs. Before analysis, the nanoparticle dispersion was sonicated for 15 min using a Vibronics VS 80 ultrasonic bath. A drop of the dispersion was placed onto a carbon-coated copper grid and allowed to dry under infrared illumination. HR-TEM analysis was performed using an FEI TECNAI T30 G2 S-TWIN transmission electron microscope operated at an accelerating voltage of 250 kV.

***Corresponding Author:**
Received: 25th May, 2026; Revised: 6th July, 2026; Accepted: 28th July, 2026; Available Online: 29th August, 2026
(DOI): 10.70102/AEJ.2026.18.8s.22

2.6.6. Selected-Area Electron Diffraction

SAED analysis was performed using the TEM system to investigate the crystalline structure of the synthesized Au-Ag BNPs. The diffraction pattern and corresponding lattice planes were evaluated to determine the crystalline nature of the nanoparticles.

2.7. In-Vitro Antioxidant Evaluation

The antioxidant potential of the synthesized Au-Ag BNPs was evaluated using DPPH, hydrogen peroxide, nitric oxide scavenging, reducing power, and total phenolic content assays. The antioxidant activity was compared with the corresponding L. inermis aqueous extract and gallic acid as the reference standard.

2.8. In-vivo evaluation in an ICV-STZ-induced mouse model

2.8.1. Animals and ethical considerations

Male and female Swiss albino mice (25-30 g; 6-8 weeks old) were used. Animals were maintained at 25 ± 2 °C and 55-65% relative humidity under a 12-h light/dark cycle, with food and water available ad libitum, and were acclimatized for 2-3 days. The source record cites CPCSEA protocol/approval number 1384. Before submission, the institutional animal ethics committee name, approval date, approved protocol number, and compliance statement must be checked against the original approval documents.

2.8.2. Induction of Alzheimer's disease-like pathology and treatment groups

An Alzheimer's disease-like phenotype was induced by intracerebroventricular (ICV) administration of streptozotocin (STZ) prepared in citrate buffer. The reported dose was 3 mg/kg, with an injection volume of 5 µL per side. The source notes injections on days 1 and 3 but also contains a conflicting dosing schedule; the actual schedule must be verified from laboratory records before submission. Donepezil (5 mg/kg, orally) was included as the reference treatment.

The six reported groups were: (I) healthy control; (II) standard-treatment control (donepezil); (III) ICV-STZ disease control; (IV) ICV-STZ + silver nanoparticles (AgNPs); (V) ICV-STZ + gold nanoparticles (AuNPs); and (VI) ICV-STZ + gold-silver bimetallic nanoparticles (Au-AgNPs). Nanoparticles were described as administered intranasally in normal saline at 48-h intervals over a 15-day treatment period. The individual doses, administration volume, number of administrations, and treatment dates were not unambiguously available in the supplied text and must be verified; they have not been inferred here.

2.8.3. Brain tissue processing and biochemical assays

At the end of the experimental period, animals were euthanized under anesthesia and brain tissue was collected for biochemical and histological evaluation. The hippocampus was isolated, rinsed with ice-cold saline, and homogenized in phosphate buffer (pH 7.4; tissue-to-buffer ratio 1:10). Homogenates were centrifuged at 800 × g for 5 min at 4 °C, and the supernatant was centrifuged at 10,500 × g for 20 min at 4 °C to obtain post-mitochondrial supernatant. A portion of brain tissue was fixed in buffered formalin for histology.

Acetylcholinesterase (AChE) and butyrylcholinesterase (BChE) activities were assessed using a modified Ellman colorimetric method with acetylthiocholine iodide or butyrylthiocholine iodide as substrate and 5,5′-dithiobis-(2-nitrobenzoic acid) (DTNB) as chromogenic reagent. Absorbance was measured at 412 nm. The enzyme calculation method, protein-normalization procedure, and final activity units should be stated from the laboratory protocol before submission.

2.8.4. ELISA measurements and histopathology

Hippocampal IL-6, IL-1β, and TNF-α were measured by ELISA. The source manuscript also reports ELISA assessment of amyloid-β1-42 (Aβ1-42), glycogen synthase kinase-3β (GSK-3β), and β-site amyloid precursor protein-cleaving enzyme 1 (BACE-1), as well as hippocampal cholesterol measurement. The exact kit manufacturers, catalogue numbers, detection ranges, and sample dilution procedures were not supplied and should be added from the experimental records. Amyloid-associated staining was examined in the hippocampal CA1 and CA3 regions using Congo red. Histological findings are treated as qualitative because quantitative plaque-area measurements were not provided.

2.8.5. Statistical analysis

Quantitative data were reported as mean ± standard error of the mean (SEM). The source describes one-way analysis of variance followed by Tukey-Kramer multiple-comparison testing, with $p < 0.05$ as the significance threshold. The number of animals contributing to each endpoint, software and version, exact adjusted p values, and the statistical output for each comparison must be verified before final submission. In the absence of the full statistical output, results below are presented descriptively and no unverified significance symbols are assigned.

3. Results and Discussion

3.1. Green Synthesis of Au-Ag Bimetallic Nanoparticles

The aqueous fraction of L. inermis leaf extract successfully facilitated the formation of Au-Ag bimetallic nanoparticles. Following the addition of the plant extract to the metal precursor solution, the reaction mixture underwent a visible color change from pale yellow to dark purple within approximately 10 min. The observed color change (shown in fig 1) can be attributed to the formation of metallic nanoparticles and the associated surface plasmon resonance phenomenon. Plant-derived phytochemicals present in the aqueous extract may act as reducing and stabilizing/capping agents, facilitating the

***Corresponding Author:**
Received: 25th May, 2026; Revised: 6th July, 2026; Accepted: 28th July, 2026; Available Online: 29th August, 2026
(DOI): 10.70102/AEJ.2026.18.8s.22

conversion of Au^{3+} and Ag^{+} ions into their corresponding metallic states. The synthesis was further optimized by evaluating four major reaction parameters: extract volume, metal precursor concentration, pH, and temperature.

3.2. Optimization of Au-Ag BNP Synthesis

3.2.1. Effect of Extract Volume

The volume of plant extract significantly influenced the formation and spectral characteristics of the Au-Ag BNPs. Different volumes of AF-LSE (10, 50, 100, 150, and 200 µL) were added to 5 mL of metal precursor solution, and nanoparticle formation was monitored for 4 h by UV-Visible spectroscopy. After 1 h, the 10 µL extract condition did not produce a clearly defined absorption peak, whereas 50 µL produced a broad peak at approximately 543 nm with an absorbance of approximately 0.8. At 100 µL, an SPR band appeared at approximately 537 nm with an absorbance of approximately 1.2. Increasing the extract volume to 150 and 200 µL resulted in SPR bands around 528 and 529 nm, respectively. After 2 h, the absorption intensity increased for most experimental conditions. At 3 h, the 100 µL condition showed only a slight increase in absorbance without substantial displacement of the SPR maximum, whereas higher extract volumes showed changes in intensity and spectral position. After 4 h, the absorption intensity at 100 µL remained comparatively stable, while higher extract volumes showed evidence of decreased intensity and/or spectral broadening as shown in fig 1.

These findings indicate that an adequate amount of plant extract is required to provide sufficient reducing and stabilizing phytochemicals. However, excessive extract concentration may alter the nucleation and growth process and may promote particle aggregation or changes in particle size distribution. Based on the observed spectral stability, 100 µL of AF-LSE was selected as the optimum extract volume for subsequent experiments.

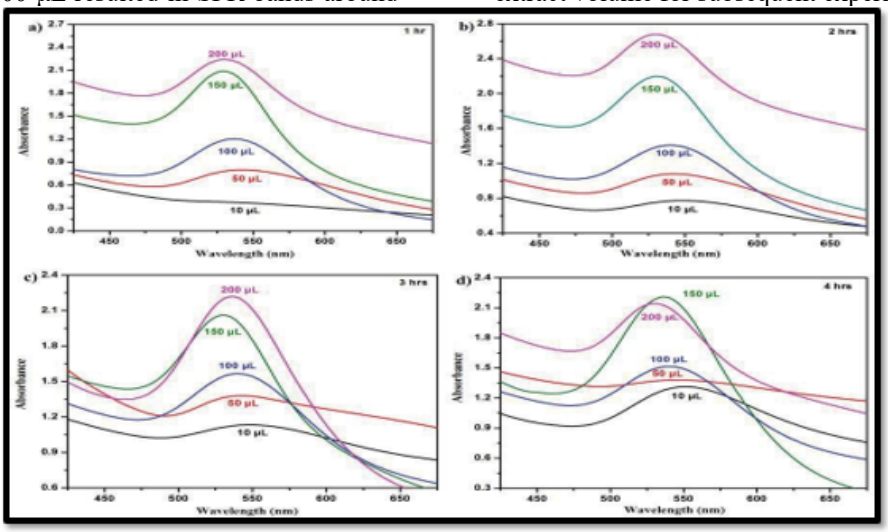


Figure 1. UV-Visible spectra showing the effect of AF-LSE volume on the synthesis of Au-Ag BNPs.

3.2.2. Effect of Metal Precursor Concentration

The influence of metal precursor concentration on Au-Ag BNP formation was investigated using 0.5, 1, 2, 3, and 4 mM precursor concentrations while maintaining the extract volume at 100 µL.

After 1 h, the 0.5 mM precursor concentration produced a broad SPR band at approximately 549 nm with an absorbance of approximately 0.48. At 1 mM, a relatively distinct SPR band appeared at approximately 537 nm with moderate absorbance. Higher precursor concentrations of 2, 3, and 4 mM produced sharper and more intense absorption bands at approximately 531, 528, and 531 nm, respectively as shown in fig 2. During prolonged reaction, the absorbance of the 0.5 and 1 mM preparations increased gradually, whereas higher precursor concentrations showed a subsequent reduction in absorption intensity. This observation suggests that excessive metal precursor concentration may accelerate nanoparticle formation but can also increase the possibility of particle growth, instability, or aggregation. The 1 mM precursor concentration demonstrated comparatively favorable spectral stability and was therefore selected for subsequent experiments.

***Corresponding Author:**
Received: 25th May, 2026; Revised: 6th July, 2026; Accepted: 28th July, 2026; Available Online: 29th August, 2026
(DOI): 10.70102/AEJ.2026.18.8s.22

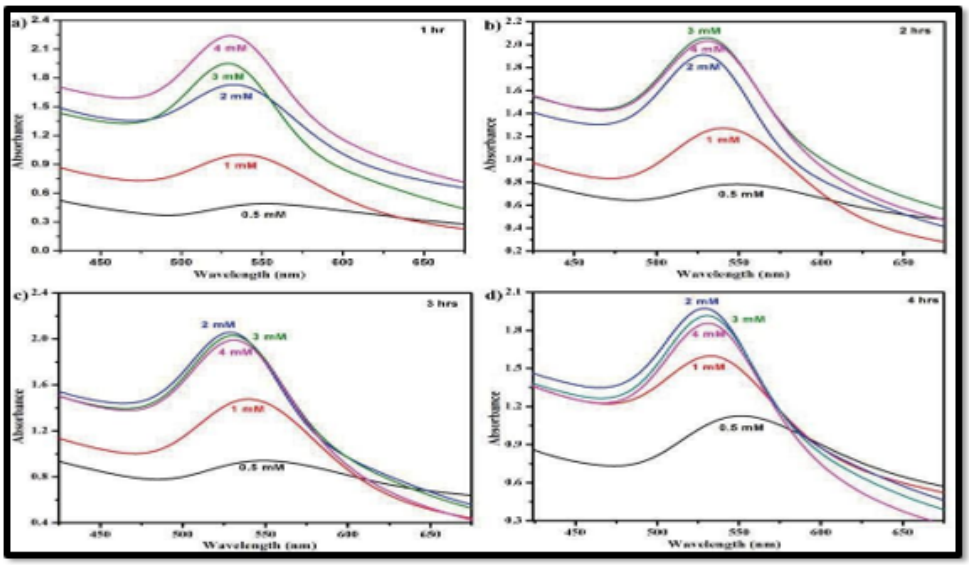


Figure 2. UV-Visible spectra showing the effect of metal precursor concentration on Au-Ag BNP synthesis.

3.2.3. Effect of pH

The pH of the reaction medium is an important parameter affecting the reduction kinetics, nucleation, growth, and stability of metallic nanoparticles. The effect of pH was therefore investigated over the range of 5-9. After 1 h, SPR bands were observed at approximately 559, 550, 540, 524, and 554 nm at pH 5, 6, 7, 8, and 9, respectively. The corresponding absorption intensities varied among the experimental conditions. At pH 5, a progressive red shift was observed during the reaction, suggesting changes in nanoparticle growth or aggregation. In contrast, the reaction at pH 7 showed comparatively stable spectral behavior, with only a minor increase in absorption intensity after prolonged incubation. At pH 8 and 9, the reduction in absorption intensity observed at later time points may indicate instability or aggregation of the nanoparticles under the experimental conditions. The results suggest that the reaction medium strongly influences the reduction kinetics and stability of the formed nanoparticles. Therefore, pH 7 was selected as the optimum condition for Au-Ag BNP synthesis.

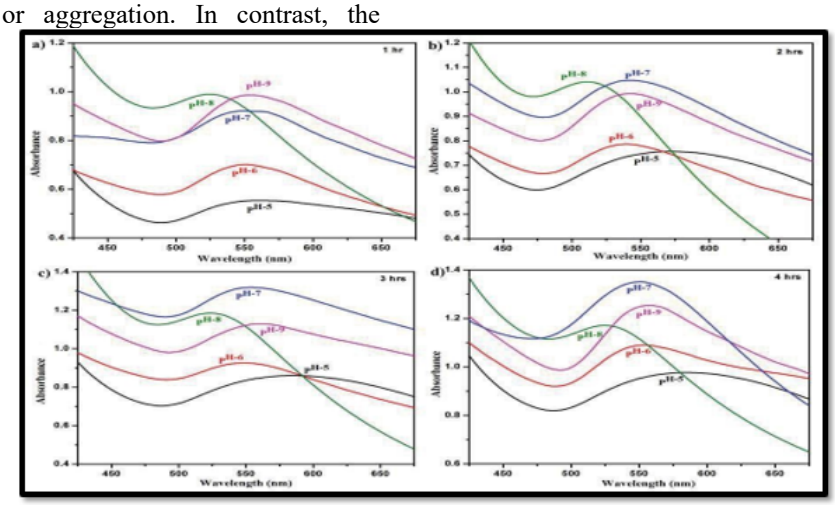


Figure 3. UV-Visible spectra showing the effect of pH on Au-Ag BNP synthesis.

3.2.4. Effect of Temperature

Temperature is another important factor affecting nanoparticle nucleation, growth kinetics, and stability. The effect of temperature was evaluated at 15, 30, 50, 70, and 80 °C. At 15 °C, no distinct SPR band was observed during the initial reaction period, indicating relatively slow nanoparticle formation. At 30 °C, a clear SPR band appeared around 540 nm with an absorbance of approximately 0.9 after 1 h as shown in fig 4. Higher temperatures produced relatively intense SPR bands during the early stages of the reaction. However, the absorption intensity subsequently decreased at 50, 70, and 80 °C. The

***Corresponding Author:**
Received: 25th May, 2026; Revised: 6th July, 2026; Accepted: 28th July, 2026; Available Online: 29th August, 2026
(DOI): 10.70102/AEJ.2026.18.8s.22

reduction in spectral intensity at higher temperatures may be associated with rapid reaction kinetics followed by particle growth and aggregation. In contrast, the reaction performed at 30 °C exhibited comparatively stable spectral behavior during the observation period. Therefore, **30 °C was selected as the optimum temperature** for Au-Ag BNP synthesis.

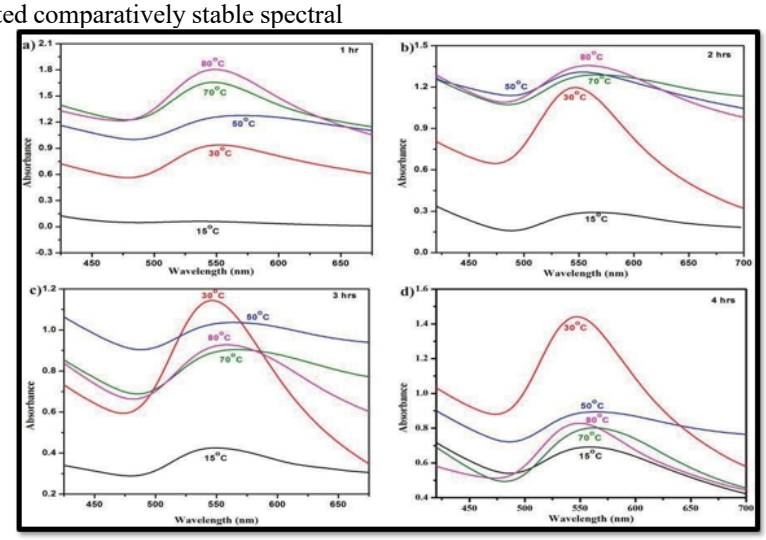


Figure 4. UV-Visible spectra showing the effect of reaction temperature on Au-Ag BNP synthesis.

3.3. Characterization of Au-Ag Bimetallic Nanoparticles

3.3.1. UV-Visible Spectroscopic Analysis

Based on the optimization studies, the optimized conditions were identified as 100 µL AF-LSE, 1 mM metal precursor, pH 7, and 30 °C. Under these conditions, Au-Ag BNPs were synthesized by sonication for 10 min. The reaction mixture gradually changed in color, confirming nanoparticle formation. The UV-Visible spectrum of the synthesized Au-Ag BNPs exhibited a distinct SPR band centered at approximately 537 nm. In contrast, the plant extract, $HAuCl_4$, $AgNO_3$, and the mixture of $HAuCl_4$ and $AgNO_3$ did not show a comparable absorption maximum in the visible region as shown in fig 5. The presence of the SPR band at 537 nm provides spectroscopic evidence for the formation of Au-Ag nanoparticles.

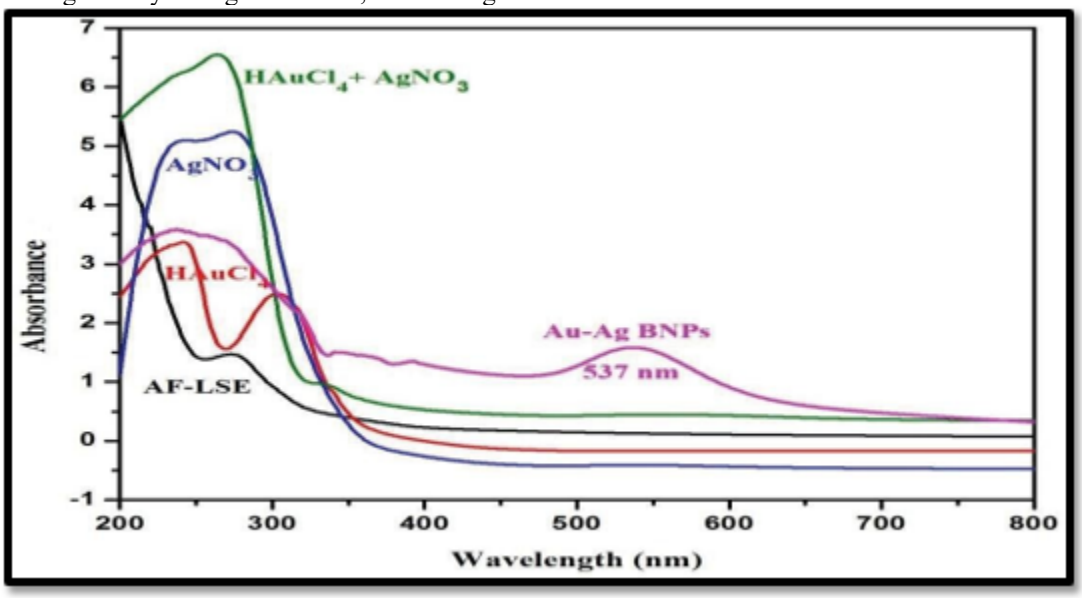


Figure 5. UV-Visible spectra of AF-LSE, $HAuCl_4$, $AgNO_3$, $HAuCl_4$ + $AgNO_3$, and synthesized Au-Ag BNPs.

The reaction kinetics were further monitored at different time intervals. The intensity of the SPR band at 537 nm increased progressively until approximately 270 min and subsequently showed no substantial change (fig 6). This observation suggests that the reduction of metal ions and nanoparticle formation approached completion by approximately 270 min under the investigated conditions.

***Corresponding Author:**
Received: 25th May, 2026; Revised: 6th July, 2026; Accepted: 28th July, 2026; Available Online: 29th August, 2026
(DOI): 10.70102/AEJ.2026.18.8s.22

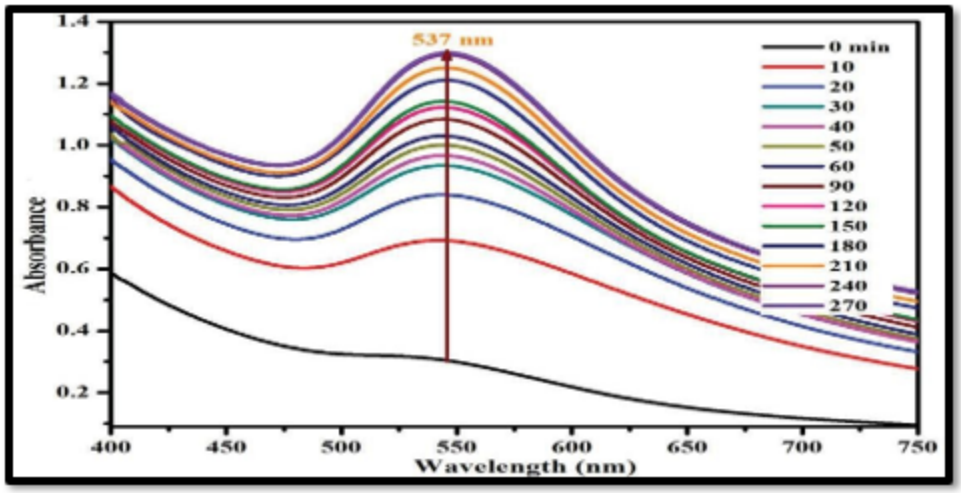


Figure 6. Time-dependent UV-Visible spectra of Au-Ag BNP synthesis.

3.3.2. FT-IR Analysis

FT-IR spectroscopy was performed to identify the functional groups present in the L. inermis extract and to investigate their possible involvement in nanoparticle reduction and stabilization.

The FT-IR spectrum of AF-LSE showed characteristic absorption bands at approximately 3454, 2984, 2888, 1649, 1484, 1411, 1337, 970, and 672 cm^{-1}. The broad band around 3454 cm^{-1} can be associated with O-H stretching vibrations of hydroxyl-containing compounds such as alcohols and phenols. The band around 2984 cm^{-1} can be attributed to C-H stretching vibrations. The band at approximately 1649 cm^{-1} may be associated with carbonyl-containing or other conjugated functional groups. Following nanoparticle synthesis, the Au-Ag BNP sample exhibited bands at approximately 3619, 2991, 2881, 1778, 1675, 1477, 1418, 1345, 962, and 660 cm^{-1} (fig 7).

The shift in several bands and changes in their relative intensities after nanoparticle synthesis suggest interactions between the phytochemicals present in the extract and the nanoparticle surface. These changes support the possible involvement of hydroxyl-, phenolic-, carbonyl-, and carboxylate-containing compounds in the reduction and stabilization of Au-Ag BNPs.

The FT-IR findings therefore suggest that phytochemicals present in L. inermis leaf extract may serve dual functions as reducing and capping/stabilizing agents during green nanoparticle synthesis.

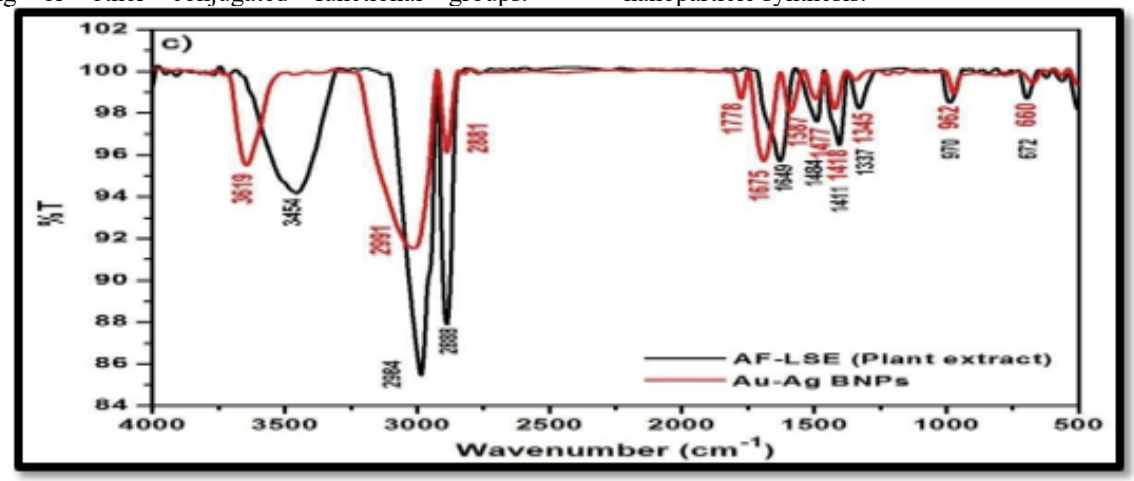


Figure 7. FT-IR spectra of AF-LSE and synthesized Au-Ag BNPs.

3.3.3. X-Ray Diffraction Analysis

XRD analysis was performed to investigate the crystalline structure of the synthesized Au-Ag BNPs. The XRD pattern exhibited characteristic diffraction peaks at approximately 38.16°, 44.43°, 64.74°, **and 77.66°**, which can be indexed to the (111), (200), (220), and (311) crystal planes, respectively, consistent with a face-centered cubic (FCC) metallic structure. The presence of these characteristic diffraction peaks confirms the crystalline nature of the synthesized nanoparticles shown in fig 8. Additional weak or unassigned reflections may be associated with crystalline or semi-crystalline organic

***Corresponding Author:**
Received: 25th May, 2026; Revised: 6th July, 2026; Accepted: 28th July, 2026; Available Online: 29th August, 2026
(DOI): 10.70102/AEJ.2026.18.8s.22

residues originating from the plant extract. Using the Scherrer equation, the average crystallite size was estimated to be approximately 38 nm. It should be noted that XRD-derived crystallite size represents the coherent crystalline domain size and may differ from the physical particle size measured by HR-TEM.

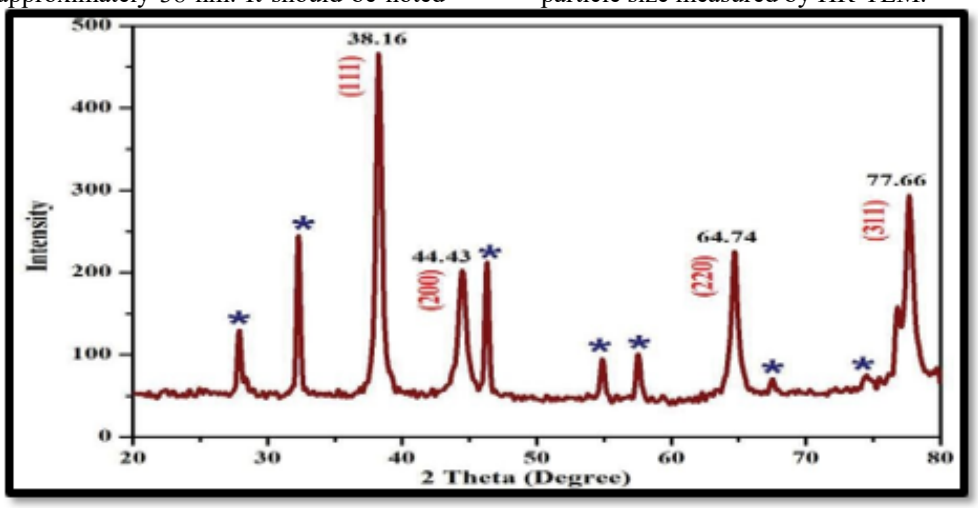


Figure 8. XRD pattern of synthesized Au-Ag BNPs.

3.3.4. EDX Analysis

EDX spectroscopy was used to determine the elemental composition of the synthesized nanoparticles. The EDX spectrum exhibited characteristic signals corresponding to both gold and silver, confirming the presence of the two metallic components. Strong Au-related signals were observed in the higher-energy region, while a characteristic Ag signal was observed around the expected Ag energy regionas shown fig 9. Additional weaker signals corresponding to carbon and oxygen were also observed, which may originate from phytochemical residues associated with the nanoparticle surface. The elemental composition obtained from the EDX analysis showed approximately 75.33 wt% Au and 18.86 wt% Ag under the reported analytical conditions. These results confirm the incorporation of both Au and Ag within the synthesized nanoparticle preparation.

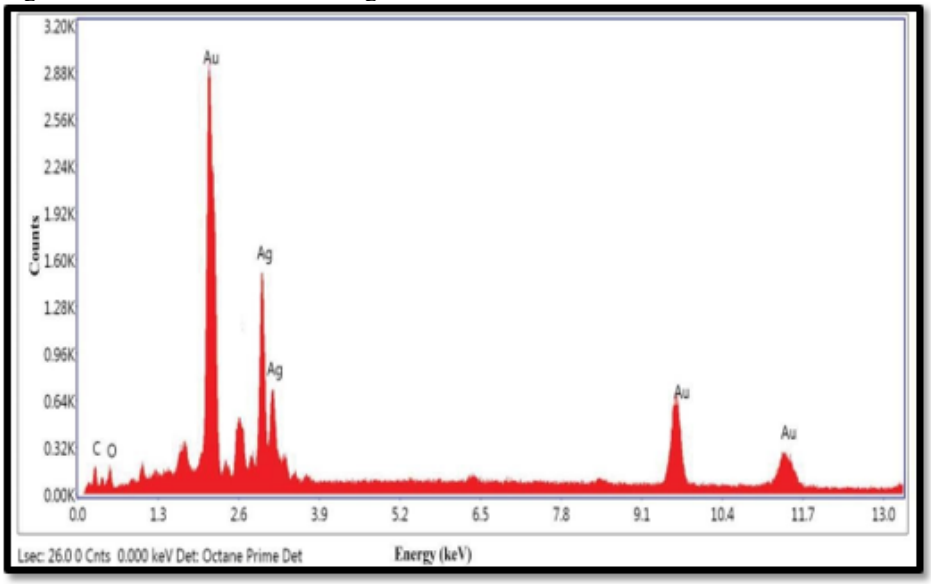


Figure 9. EDX spectrum of synthesized Au-Ag BNPs.

3.3.5. HR-TEM Analysis

HR-TEM was performed to determine the morphology and approximate particle size of the synthesized Au-Ag BNPs. The TEM micrographs obtained at different magnifications revealed nanoparticles with predominantly spherical, polygonal, and irregular morphologies. The observed particle sizes were approximately 10-32 nm. The nanoparticles appeared relatively well dispersed in the representative micrographs, although the possibility of localized aggregation cannot be excluded. The nanoscale

***Corresponding Author:**
Received: 25th May, 2026; Revised: 6th July, 2026; Accepted: 28th July, 2026; Available Online: 29th August, 2026
(DOI): 10.70102/AEJ.2026.18.8s.22

particle dimensions observed by HR-TEM are consistent with the formation of nanostructured Au-Ag particles as shown in fig 10. The difference between the HR-TEM particle size range and the XRD-derived crystallite size may be attributed to differences between physical particle dimensions and crystalline domain dimensions.

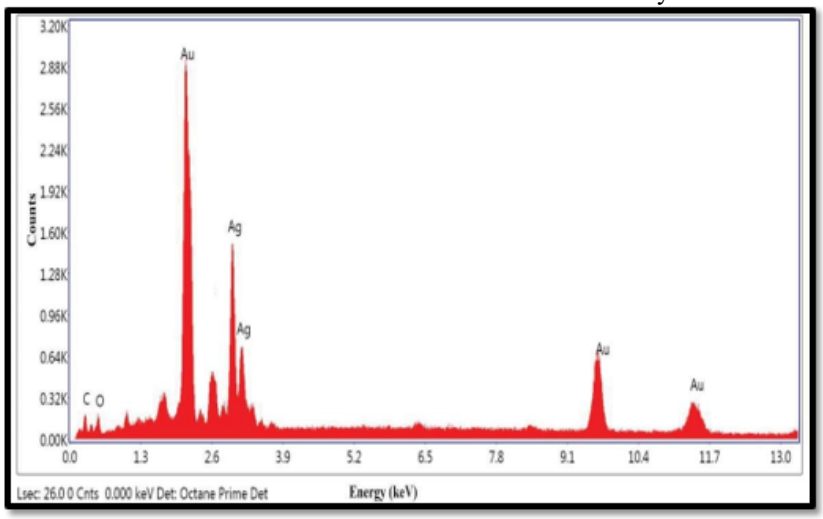


Figure 10. HR-TEM images of synthesized Au-Ag BNPs at different magnifications.

3.3.6. Evidence for the Bimetallic Nature of Au-Ag BNPs

Bimetallic nanoparticles may exist in different structural arrangements, including alloy and core-shell configurations. Optical spectroscopy can provide preliminary information regarding nanoparticle structure, although definitive differentiation between alloy and core-shell architectures generally requires additional techniques such as elemental mapping, STEM-EDS, XPS, or other advanced structural analyses. In the present study, a single broad SPR band centered at approximately 537 nm was observed for the synthesized Au-Ag BNPs. The presence of a single SPR band is consistent with the formation of a bimetallic system and may support an alloy-like structure. However, UV-Visible spectroscopy alone is not sufficient to definitively establish an alloy architecture. The EDX analysis confirmed the simultaneous presence of Au and Ag, with approximately 75.33 wt% Au and 18.86 wt% Ag. These findings demonstrate that both metals were incorporated into the synthesized nanoparticle preparation. Therefore, the synthesized material can appropriately be described as Au-Ag bimetallic nanoparticles, while definitive confirmation of an alloy versus core-shell architecture would require additional structural characterization.

3.4. In-Vitro Antioxidant Activity

The antioxidant potential of the synthesized Au-Ag BNPs was evaluated using DPPH, H_2O_2, NO scavenging, reducing power, and total phenolic content assays. The activity was compared with AF-LSE and gallic acid.

3.4.1. DPPH Radical Scavenging Activity

The DPPH radical scavenging assay was used to investigate the free-radical scavenging capacity of the synthesized nanoparticles. DPPH is a stable nitrogen-centered free radical that exhibits a characteristic purple color. Reduction of DPPH by antioxidant compounds results in a decrease in absorbance. The synthesized Au-Ag BNPs demonstrated concentration-dependent DPPH radical scavenging activity. At concentrations of 10, 20, 40, 60, 80, and 100 µg/mL, the percentage inhibition obtained with Au-Ag BNPs was 41.73, 49.72, 60.49, 71.30, 79.53, and 88.78%, respectively. At 100 µg/mL, the Au-Ag BNPs exhibited higher DPPH scavenging activity than both AF-LSE (80.76%) and gallic acid (83.01%) (table 1). The increased activity of the nanoparticles may be associated with the combined contribution of phytochemical residues associated with the nanoparticle surface and the physicochemical characteristics of the bimetallic system.

Table 1. DPPH radical scavenging activity of AF-LSE, Au-Ag BNPs, and gallic acid

Concentration (µg/mL)	AF-LSE (%)	Au-Ag BNPs (%)	Gallic acid (%)
10	30.77	41.73	39.22
20	40.68	49.72	47.26
40	49.87	60.49	55.51
60	58.43	71.30	67.60
80	69.86	79.53	75.66
100	80.76	88.78	83.01

***Corresponding Author:**
Received: 25th May, 2026; Revised: 6th July, 2026; Accepted: 28th July, 2026; Available Online: 29th August, 2026
(DOI): 10.70102/AEJ.2026.18.8s.22

3.4.2. Hydrogen Peroxide Scavenging Activity

Hydrogen peroxide is an important reactive oxygen species that can participate in oxidative processes and generate highly reactive hydroxyl radicals in the presence of suitable transition-metal ions. The H_2O_2 scavenging assay was therefore used to evaluate the antioxidant potential of the synthesized nanoparticles. The Au-Ag BNPs demonstrated concentration-dependent H_2O_2 scavenging activity. At 100 µg/mL, the percentage inhibition was **90.03%**, compared with 79.54% for AF-LSE and 72.51% for gallic acid (table 2). The higher activity observed with Au-Ag BNPs suggests that the synthesized nanoparticle preparation possesses considerable H_2O_2 scavenging potential under the experimental conditions.

Table 2. H_2O_2 scavenging activity of AF-LSE, Au-Ag BNPs, and gallic acid

Concentration (µg/mL)	AF-LSE (%)	Au-Ag BNPs (%)	Gallic acid (%)
10	26.06	38.23	22.51
20	35.50	49.19	33.95
40	46.39	60.76	44.46
60	61.88	72.01	58.37
80	70.13	80.11	64.28
100	79.54	90.03	72.51

3.4.3. Nitric Oxide Scavenging Activity

Nitric oxide is an important signaling molecule; however, excessive NO production under pathological conditions may contribute to oxidative and inflammatory processes. The NO scavenging assay was therefore performed to evaluate the potential of the synthesized nanoparticles to inhibit nitrite formation. The Au-Ag BNPs exhibited concentration-dependent NO scavenging activity. At 100 µg/mL, the percentage inhibition was **88.08%**, compared with 78.97% for AF-LSE and 75.85% for gallic acid (table 3). The enhanced NO scavenging activity observed for the Au-Ag BNPs indicates a potentially greater radical-scavenging capacity of the nanoparticle preparation under the experimental conditions.

Table 3. Nitric oxide scavenging activity of AF-LSE, Au-Ag BNPs, and gallic acid

Concentration (µg/mL)	AF-LSE (%)	Au-Ag BNPs (%)	Gallic acid (%)
10	25.74	36.17	24.57
20	35.45	47.88	33.79
40	47.65	55.01	42.23
60	59.46	64.38	54.33
80	67.60	78.47	66.49
100	78.97	88.08	75.85

3.4.4. Reducing Power Activity

The ferric reducing power assay was performed to evaluate the electron-donating/reducing capacity of the samples. An increase in absorbance at 700 nm indicates greater reducing capacity.

The reducing power of all samples increased with increasing concentration. At 100 µg/mL, the reported absorbance values were 0.1821 for AF-LSE, 0.193 for Au-Ag BNPs, and 0.1852 for gallic acid (table 4). The Au-Ag BNPs showed the highest reducing activity among the three tested samples. This result is consistent with the radical-scavenging assays and indicates that the nanoparticle preparation possesses appreciable electron-donating capacity.

Table 4. Reducing power activity of AF-LSE, Au-Ag BNPs, and gallic acid

Concentration (µg/mL)	AF-LSE (%)	Au-Ag BNPs (%)	Gallic acid (%)
10	25.01	38.31	20.02
20	38.92	50.20	29.37
40	52.03	62.80	40.65
60	64.13	75.61	57.62
80	76.02	85.37	70.02
100	88.21	95.14	85.06

3.4.5. Total Phenolic Content

The total phenolic content (TPC) of AF-LSE and Au-Ag BNPs was determined using the Folin-Ciocalteu method, with gallic acid used as the reference standard. The calibration curve obtained (fig 11B) using gallic acid showed a linear relationship described by the equation:

***Corresponding Author:**
Received: 25th May, 2026; Revised: 6th July, 2026; Accepted: 28th July, 2026; Available Online: 29th August, 2026
(DOI): 10.70102/AEJ.2026.18.8s.22

y = 0.0078x + 0.1416
with an **R² value of 0.9901**, indicating a strong linear relationship within the investigated concentration range. At the reported concentration, the TPC values were approximately **45.6 mg GAE/g for AF-LSE and 35.4 mg GAE/g for Au-Ag BNPs**.
The lower measured TPC of the nanoparticle preparation compared with the extract may reflect the utilization, adsorption, or modification of phenolic constituents during the reduction and stabilization of the metal ions (table 5 fig 11A). Nevertheless, the detection of phenolic-associated reducing capacity in the nanoparticle preparation supports the possible involvement of plant-derived phytochemicals during nanoparticle synthesis.

Table 5. Total phenolic content of AF-LSE and Au-Ag BNPs

Concentration (µg/mL)	AF-LSE (mg GAE/g)	Au-Ag BNPs (mg GAE/g)
10	16.0	6.6
20	21.6	8.8
40	26.6	12.0
60	32.2	14.4
80	39.4	17.6
100	45.6	35.4

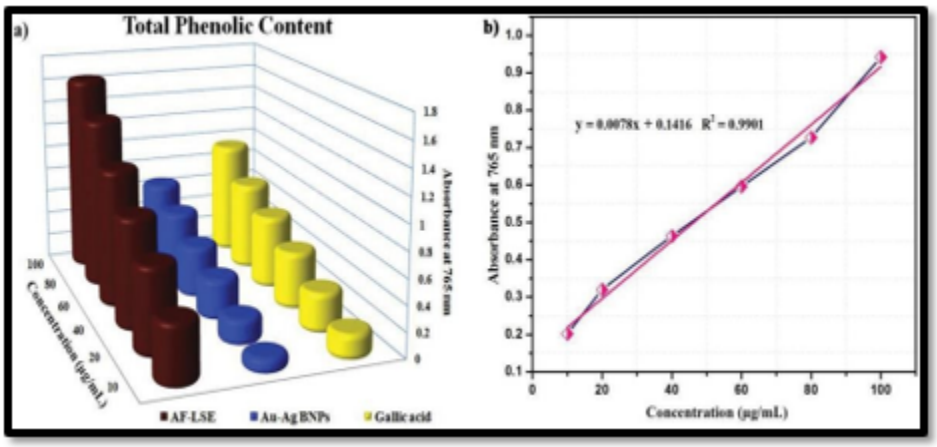


Figure 11. (A) Comparative phenolic content of AF-LSE and Au-Ag BNPs; (B) calibration curve of gallic acid.

3.5. In-vivo findings in the ICV-STZ mouse model

3.5.1. Cholinesterase activity

ICV-STZ was associated with higher hippocampal cholinesterase activity than the healthy-control condition. AChE activity increased from 7.384 ± 1.13 in healthy controls to 17.42 ± 0.51 in the disease-control group, while BChE increased from 0.018 ± 0.0017 to 0.029 ± 0.0021. The Au-AgNP group showed AChE and BChE values of 7.21 ± 0.22 and 0.018 ± 0.0002, respectively, numerically close to the healthy-control values. Units are reproduced from the source and require confirmation.

Table 6. Hippocampal AChE and BChE activity across experimental groups.

Group	AChE activity	BChE activity
Healthy control	7.384 ± 1.13	0.018 ± 0.0017
Standard treatment (donepezil)	7.85 ± 0.60	0.019 ± 0.0024
ICV-STZ disease control	17.42 ± 0.51	0.029 ± 0.0021
ICV-STZ + AgNPs	9.51 ± 0.51	0.020 ± 0.0012
ICV-STZ + AuNPs	7.33 ± 0.52	0.019 ± 0.0016
ICV-STZ + Au-AgNPs	7.21 ± 0.22	0.018 ± 0.0002

The numerical pattern suggests that Au-AgNP treatment was associated with the greatest normalization of the two reported cholinesterase measures among nanoparticle-treated groups. Pairwise statistical significance cannot be established from the supplied summary alone.

***Corresponding Author:**
Received: 25th May, 2026; Revised: 6th July, 2026; Accepted: 28th July, 2026; Available Online: 29th August, 2026
(DOI): 10.70102/AEJ.2026.18.8s.22

3.5.2. Hippocampal inflammatory cytokines

The disease-control group showed higher IL-6, IL-1β, and TNF-α concentrations than healthy controls. The Au-AgNP group showed values close to those of the healthy controls across all three cytokines. Concentrations are reported as mean ± SEM in pg/mL.

Table 7. Hippocampal inflammatory cytokine concentrations across experimental groups.

Group	IL-6 (pg/mL)	IL-1β (pg/mL)	TNF-α (pg/mL)
Healthy control	29.78 ± 2.26	48.38 ± 2.25	124.9 ± 2.77
Standard treatment	32.24 ± 2.28	49.26 ± 3.22	135.4 ± 5.97
ICV-STZ disease control	45.13 ± 1.99	71.40 ± 2.86	191.0 ± 12.67
ICV-STZ + AgNPs	34.10 ± 1.18	59.36 ± 2.29	153.3 ± 4.36
ICV-STZ + AuNPs	30.34 ± 1.41	49.25 ± 2.33	134.6 ± 2.30
ICV-STZ + Au-AgNPs	29.34 ± 1.41	48.55 ± 2.33	124.6 ± 2.30

The consistent reduction across the three cytokines is compatible with an association between nanoparticle treatment and lower hippocampal inflammatory-marker concentrations. These observations do not identify a specific molecular mechanism.

3.5.3. Hippocampal cholesterol

Hippocampal cholesterol was higher in the ICV-STZ disease-control group (156.6 ± 6.322 µg/mL) than in healthy controls (115.5 ± 3.214 µg/mL). The AgNP-, AuNP-, and Au-AgNP-treated groups showed values of 125.7 ± 5.876, 120.2 ± 5.386, and 116.5 ± 5.235 µg/mL, respectively. The Au-AgNP value was numerically closest to the healthy-control value.

Table 8. Hippocampal cholesterol concentrations across experimental groups.

Group	Hippocampal cholesterol (µg/mL)
Healthy control	115.5 ± 3.214
ICV-STZ disease control	156.6 ± 6.322
ICV-STZ + AgNPs	125.7 ± 5.876
ICV-STZ + AuNPs	120.2 ± 5.386
ICV-STZ + Au-AgNPs	116.5 ± 5.235

3.5.4. Amyloid-associated biomarkers and histology

Aβ1-42 was reported at 515.5 ± 2.219 pg/mL in healthy controls and 796.6 ± 6.349 pg/mL in the ICV-STZ disease-control group. The AgNP group was reported at 535.7 ± 6.891 pg/mL. The supplied material describes lower Aβ1-42 values after AuNP and Au-AgNP treatment but does not provide their complete numerical results; those values are therefore not reproduced or estimated here. Congo red-stained sections were described as showing greater amyloid-associated staining in CA1 and CA3 in the disease-control group and visibly reduced staining in nanoparticle-treated groups. Because quantitative plaque-area or blinded histological scores were not supplied, these observations are qualitative.

GSK-3β was reported at 4.60 ± 0.22 ng/mL in healthy controls, 7.98 ± 0.54 ng/mL in the disease-control group, and 4.74 ± 0.60 ng/mL in the standard-treatment group. The complete nanoparticle-group values were not available in the supplied data. BACE-1 was reported at 23.8 ± 12.13 ng/mL in healthy controls, 24.7 ± 10.77 ng/mL in the standard-treatment group, 31.3 ± 18.00 ng/mL in the disease-control group, and 23.9 ± 32.18 ng/mL in the Au-AgNP group. The unusually large SEM for the latter value should be checked against the raw dataset before interpretation.

3.5.5. Summary of in-vivo observations

Across the reported endpoints, Au-AgNP treatment was associated with lower cholinesterase activity, lower hippocampal cytokine concentrations, and a hippocampal cholesterol value close to the healthy-control value. The available data also describe reductions in amyloid-associated measures, but some biomarker values and statistical outputs are incomplete. These findings are preliminary biochemical and histological observations; behavioural efficacy, nanoparticle safety, brain exposure, and disease-modifying effects cannot be concluded from the supplied results.

4. Discussion

The present work combines green synthesis and physicochemical characterization of Lawsonia inermis-mediated Au-Ag bimetallic nanoparticles with in-vitro antioxidant assays and a preliminary in-vivo evaluation reported in an ICV-STZ mouse model. The optimized synthesis conditions-100 µL aqueous leaf fraction, 1 mM metal precursor, pH 7, and 30 °C-produced a UV-visible absorption band at approximately 537 nm. FT-IR band changes suggest that plant-derived functional groups may interact with the nanoparticle surface, while XRD support a crystalline face-centred cubic structure. HR-TEM showed particles approximately 10-32 nm in size; the

***Corresponding Author:**
Received: 25th May, 2026; Revised: 6th July, 2026; Accepted: 28th July, 2026; Available Online: 29th August, 2026
(DOI): 10.70102/AEJ.2026.18.8s.22

larger Scherrer estimate reflects a different measurement of crystalline domain size and should not be interpreted as a direct contradiction.

EDX detected both gold and silver in the nanoparticle preparation. However, the available EDX and UV-visible data do not definitively distinguish an alloy from a core-shell architecture. Elemental mapping, STEM-EDS, XPS, or complementary structural methods would be needed to establish the spatial arrangement and oxidation state of the two metals. The reported Au and Ag weight percentages should also be checked against the original EDX output, including the contribution of other detected elements.

The in-vitro assays showed concentration-dependent activity in DPPH, hydrogen-peroxide and nitric-oxide scavenging tests, as well as increased reducing capacity. At 100 µg/mL, Au-AgNPs produced reported inhibition values of 88.78% for DPPH, 90.03% for H_2O_2, and 88.08% for nitric oxide. These results indicate activity under the assay conditions but do not by themselves demonstrate antioxidant efficacy in biological systems. Nanoparticle-only blanks, assay interference controls, replicate numbers, dispersion measures, and IC_{50} estimates should be reported where available. The total phenolic content values also require careful interpretation because the nanoparticle matrix may influence Folin-Ciocalteu response and the reported concentration-dependent values should be reconciled with the stated units.

The in-vivo summary shows that the ICV-STZ disease-control group had higher AChE and BChE activity, inflammatory cytokines, hippocampal cholesterol, and Aβ1-42 than healthy controls. Au-AgNP treatment was associated with values closer to healthy controls for cholinesterase activity, IL-6, IL-1β, TNF-α, and cholesterol. These numerical patterns are consistent with a possible biological effect, but no causal mechanism or therapeutic benefit can be established without complete group-level data, confirmed sample sizes, full statistical output, and independent replication. Aβ1-42 values for all nanoparticle groups and the full GSK-3β dataset were not available in the supplied material; no missing values have been inferred.

An important distinction is that the in-vivo section supplied for integration describes intranasal nanoparticle preparations in an ICV-STZ mouse model. It does not establish that an Au-AgNP-loaded mucoadhesive in-situ gel was evaluated in that experiment. Consequently, the present manuscript should not claim that the gel formulation improves nose-to-brain delivery unless formulation characterization, mucoadhesion, gelation, drug release, nasal tolerability, pharmacokinetics, and brain-distribution data are available. Intranasal administration alone is not evidence of nose-to-brain targeting.

Several limitations should be addressed before journal submission. The animal dosing schedule is inconsistent in the source material, and nanoparticle doses, administration volumes, exact treatment dates, animal numbers, and the formal ethics approval details need verification. The units for cholinesterase activity, enzyme normalization, ELISA kit details, and the high SEM reported for BACE-1 should be checked against raw records. The supplied in-vivo data do not include behavioural testing or quantitative histological analysis. These gaps limit reproducibility and prevent strong claims regarding cognitive improvement or disease modification.

5. Conclusion

The aqueous leaf fraction of Lawsonia inermis supported green synthesis of Au-Ag bimetallic nanoparticles under optimized conditions of 100 µL extract, 1 mM metal precursor, pH 7, and 30 °C. UV-visible spectroscopy showed an absorption band near 537 nm; FT-IR suggested interactions between plant-derived functional groups and the nanoparticle surface; and XRD, EDX, HR-TEM, and SAED provided complementary evidence of crystalline nanoscale material containing both Au and Ag. The preparation showed concentration-dependent in-vitro antioxidant activity.

The supplied ICV-STZ mouse data further showed that intranasal nanoparticle treatment-particularly Au-AgNPs-was associated with changes in cholinesterase activity, hippocampal cytokines, and cholesterol. These results are preliminary and should be interpreted in light of incomplete dosing details, missing biomarker values, and the need to verify sample sizes and statistical analyses. The current evidence does not demonstrate cognitive benefit, definitive nose-to-brain targeting, or efficacy of an Au-AgNP-loaded in-situ gel. Further work should include complete formulation development, nasal safety, pharmacokinetics and brain distribution, behavioural testing, and fully reported, independently replicated animal experiments.

References

1. Xu Y, Ye X, Du Y, Yang W, Tong F, Li W, et al. Nose-to-brain delivery of targeted lipid nanoparticles as two-pronged β-amyloid nanoscavenger for Alzheimer's disease therapy. Acta Pharm Sin B. 2025;15(6):2884-2899. doi:10.1016/j.apsb.2025.02.035.
2. Li WB, Xu LL, Wang SL, Wang YY, Pan YC, Shi LQ, et al. Co-assembled nanoparticles toward multi-target combinational therapy of Alzheimer's disease by making full use of molecular recognition and self-assembly. Adv Mater. 2024;36(28):e2401918. doi:10.1002/adma.202401918.
3. He X, Peng Y, Huang S, Xiao Z, Li G, Zuo Z, et al. Blood brain barrier-crossing delivery of felodipine nanodrug ameliorates anxiety-like behavior and cognitive impairment in Alzheimer's disease. Adv Sci (Weinh). 2024;11(34):e2401731. doi:10.1002/advs.202401731.
4. Huang Q, Chen Y, Zhang W, Xia X, Li H, Qin M,

***Corresponding Author:**

Received: 25th May, 2026; Revised: 6th July, 2026; Accepted: 28th July, 2026; Available Online: 29th August, 2026
(DOI): 10.70102/AEJ.2026.18.8s.22

et al. Nanotechnology for enhanced nose-to-brain drug delivery in treating neurological diseases. J Control Release. 2024;366:519-534. doi:10.1016/j.jconrel.2023.12.054.
5. Chen Y, Zhang C, Huang Y, Ma Y, Song Q, Chen H, et al. Intranasal drug delivery: the interaction between nanoparticles and the nose-to-brain pathway. Adv Drug Deliv Rev. 2024;207:115196. doi:10.1016/j.addr.2024.115196.
6. Boyetey MJB, Choi Y, Lee HY, Choi J. Nanotechnology-based delivery of therapeutics through the intranasal pathway and the blood-brain barrier for Alzheimer's disease treatment. Biomater Sci. 2024;12(8):2007-2018. doi:10.1039/D3BM02003G.
7. Sharma S, Tyagi A, Dang S. Nose to brain delivery of transferrin conjugated PLGA nanoparticles for clonidine. Int J Biol Macromol. 2023;252:126471. doi:10.1016/j.ijbiomac.2023.126471.
8. Akilandaeaswari B, Muthu K. One-pot green synthesis of Au-Ag bimetallic nanoparticles from Lawsonia inermis seed extract and its catalytic reduction of environmental polluted methyl orange and 4-nitrophenol. J Taiwan Inst Chem Eng. 2021;127:292-301. doi:10.1016/j.jtice.2021.07.019.
9. Akilandaeaswari B, Muthu K. Green method for synthesis and characterization of gold nanoparticles using Lawsonia inermis seed extract and their photocatalytic activity. Mater Lett. 2020;277:128344. doi:10.1016/j.matlet.2020.128344.
10. Kumari P, Meena A. Green synthesis of gold nanoparticles from Lawsonia inermis and its catalytic activities following the Langmuir-Hinshelwood mechanism. Colloids Surf A Physicochem Eng Asp. 2020;606:125447. doi:10.1016/j.colsurfa.2020.125447.
11. Alhomaidi E, Jasim SA, Amin HIM, Nobre MAL, Khatami M, Jalil AT, et al. Biosynthesis of silver nanoparticles using Lawsonia inermis and their biomedical application. IET Nanobiotechnol. 2022;16(7-8):284-294. doi:10.1049/nbt2.12096.
12. Moosavy MH, de la Guardia M, Mokhtarzadeh A, Khatibi SA, Hosseinzadeh N, Hajipour N, et al. Green synthesis, characterization, and biological evaluation of gold and silver nanoparticles using Mentha spicata essential oil. Sci Rep. 2023;13:7230. doi:10.1038/s41598-023-33632-y.
13. Thirumoorthy G, Balasubramanian B, George JA, Nizam A, Nagella P, Srinatha N, et al. Phytofabricated bimetallic synthesis of silver-copper nanoparticles using Aerva lanata extract to evaluate their potential cytotoxic and antimicrobial activities. Sci Rep. 2024;14:1270. doi:10.1038/s41598-024-51647-x.
14. Ghasemi S, Dabirian S, Kariminejad F, Eghbali Koohi D, Nemattalab M, Majidimoghadam S, et al. Process optimization for green synthesis of silver nanoparticles using Rubus discolor leaves extract and its biological activities against multi-drug resistant bacteria and cancer cells. Sci Rep. 2024;14:4130. doi:10.1038/s41598-024-54702-9.
15. Velidandi A, Sarvepalli M, Gandam PK, Baadhe RR. Silver/silver chloride and gold bimetallic nanoparticles: green synthesis using Azadirachta indica aqueous leaf extract, characterization, antibacterial, catalytic, and recyclability studies. Inorg Chem Commun. 2023;155:111107. doi:10.1016/j.inoche.2023.111107.
16. Selim S, Badr BM, Moustafa MH, Saied E, Elkady FM, Salama A, et al. Green biosynthesis of bimetallic silver titanium dioxide nanoparticles using Pluchea indica with their anticancer, antimicrobial, and antioxidant activities. Sci Rep. 2025;15:26735. doi:10.1038/s41598-025-10349-8.
17. Bohdanovych T, Kuzema P, Anishchenko V, Duplij V, Kharchuk M, Lyzhniuk V, et al. Comparison of silver and gold nanoparticles green synthesis by Artemisia annua hairy root extracts. Biol Open. 2025;14(3):bio061739. doi:10.1242/bio.061739.
18. Arroyo G, Angulo Y, Naranjo B, Toscano F, Torres Arias M, Debut A, et al. Green synthesis of antioxidant and low-toxicity gold and silver nanoparticles using floral extracts. OpenNano. 2025;26:100258. doi:10.1016/j.onano.2025.100258.
19. Khalil AMA, Saied E, Mekky AE, Saleh AM, et al. Green biosynthesis of bimetallic selenium-gold nanoparticles using Pluchea indica leaves and their biological applications. Front Bioeng Biotechnol. 2024;11:1294170. doi:10.3389/fbioe.2023.1294170.
20. Martins GR, Monteiro AF, Amaral FRL, Silva AS. A validated Folin-Ciocalteu method for total phenolics quantification of condensed tannin-rich açaí (Euterpe oleracea Mart.) seeds extract. J Food Sci Technol. 2021;58(12):469**3-4702. doi:10.1007/s13197-020-04959-5.**

***Corresponding Author:**
Received: 25th May, 2026; Revised: 6th July, 2026; Accepted: 28th July, 2026; Available Online: 29th August, 2026
(DOI): 10.70102/AEJ.2026.18.8s.22